Effects of dynamic induction control on power and loads, by LES-ALM simulations and wind tunnel experiments

C Wang[1], F Campagnolo[1], A Sharma[2] and C L Bottasso[1]

[1]Wind Energy Institute, Technische Universität München, Boltzmannstraße 15, D-85748 Garching bei München, Germany

[2]Fraunhofer IWES, Fraunhofer Institute for Wind Energy Systems, Am Seedeich 45, D-27572 Bremerhaven, Germany

E-mail: carlo.bottasso@tum.de

Abstract.

Dynamic Induction Control (DIC) has the potential of boosting wind farm power by enhancing wake recovery, whereby periodic pitch motions are used to exploit the natural instabilities of wind turbine wakes. This work studies DIC both experimentally and numerically. A thorough validation of an LES-ALM (Actuator Line Method) simulation tool is first conducted against experimental measurements. This shows that the CFD model is able to accurately simulate the power, loads and wake behavior of a wind turbine operating with DIC. The validated CFD model is then employed to study the effects of some DIC parameters. Results indicate an increase in the fatigue loads caused by the pitch activity that enhances wake recovery.

1. Introduction

Wake effects reduce power output and increase loading in wind farms. Various strategies have been proposed and explored to mitigate the adverse impacts of wakes. Recently, a novel Dynamic Induction Control (DIC) strategy has been proposed and studied by LES-AD (Actuator Disk) simulations [1, 2]. The strategy exploits the natural instabilities in the near-wake vortex structures to enhance wake recovery. The technique works by sinusoidally varying the rotor thrust in open-loop; when performed at the right frequency, this perturbation has the effect of speeding up vortex breakdown and the recovery of the wake. This strategy results in a power increase for the downstream turbine that exceeds the power loss on the upstream one, so that the combined upstream-downstream power increases. The potential of DIC has been demonstrated in [3] through wind tunnel experiments and CFD-AD simulations, although the observed increase in wind farm power was not as high as the one found in [1, 2]. In addition, a first assessment of the effects of DIC on loads was attempted by aeroelastic simulations [3] based on a Blade-Element Momentum (BEM) method, i.e., without considering a complete CFD simulation of the system.

To the present date, it appears that the effects of DIC on power and loads have not yet been demonstrated by a CFD-ALM simulation. The present paper aims to fill this gap.

This work first verifies the accuracy of an LES-ALM solver when applied to DIC. The underlying idea is that the more accurate representation of the rotor and near wake behavior offered by ALM, when compared to AD, might lead to a better and more detailed representation

of the physical processes that govern dynamic induction. The verification of the simulation model is here accomplished with the help of wind tunnel experiments performed with scaled wind turbines [3]. After showing a good match between CFD and the experimental data, the validated LES-ALM tool is exploited to further characterize and optimize dynamic induction control in terms of wind farm power. Finally, loads of the optimized DIC case are compared to the ones of the baseline case without DIC, showing a significant impact of this control strategy on fatigue.

2. Methodology

2.1. Experimental setup

A cluster of three aligned wind turbines of the G1 type [4, 5] was operated in the boundary layer wind tunnel of the Politecnico di Milano, with a longitudinal spacing of 5D. The inflow turbulence intensity was about 5%. Turbulence was generated passively by using spires close to the inlet of the wind tunnel test section. The wind tunnel has a cross-section of 3.8×13.8 m^2, sufficient to avoid significant blockage effects [6]. A pitot probe was placed 2.3 D upstream of the first turbine to record the inflow conditions.

2.2. Numerical model

The LES flow solver is based on Foam-extend [7], while the wind turbine and farm models are implemented in FAST [8] and SOWFA [9], respectively. The software has been validated in previous work [10]. Both LES and faster scale adaptive simulation (SAS) [11] methods have been used for the various cases considered here. Although the results of both turbulence models are very close, SAS can be used on coarser meshes, hence reducing the computational time. A passive turbulence generation method with a cluster of spires was applied in the wind tunnel. This physical process was simulated with CFD using a structured body-conforming mesh of the spires [12]. The mean wind speed, turbulence intensity and vertical shear were validated with hot-wire measurements performed in the tunnel. The turbulent flow was sampled on a plane 3.8 D in front of the first turbine for every time-step, and then used as inflow for the subsequent LES-ALM wind turbine simulations. The same inflow data has been used for all CFD cases.

2.3. Wind turbine control

In all experiments and simulations, DIC is only applied to the first turbine since there is apparently no gain when also applied to the intermediate one [2]. The collective blade pitch angle β is the sinusoidal function

$$\beta = \alpha + A\sin(ft), \tag{1}$$

where α is the steady pitch angle, A is the dynamic pitch amplitude, and f is its frequency. Changing α corresponds to the classical axial induction control, in which the thrust of upstream turbines is decreased in order to increase the power of downstream machines. The frequency f is related to the Strouhal number $St = fD/U_\infty$, which has a significant effect on the recovery of the wake and, hence, on wind farm power [3]. The two downstream turbines are governed by standard PI torque controllers, and their pitch angles are always equal to the fine pitch angle, which is 0.4° for the G1 turbine.

3. Results

3.1. CFD validation: single-turbine cases

Comparisons between CFD and experiments are conducted with respect to the wake profile of the first turbine, to the power and thrust of both the upstream and downstream turbines and their sensitivity to DIC parameters. For the purpose of wake comparison, only the first turbine was operated in the wind tunnel, and its wake 5D downstream was measured with hot-wire probes in different operating conditions. Figure 1 shows the hub-height time-averaged lateral wake profiles. The static pitch angle α and dynamic amplitude A cover a fairly wide range,

and for each operating condition, the agreement between experiments and simulations is good. Case 1, shown on the left of Fig. 1, has a relatively high pitch amplitude, and it is termed "the reference case" in the following.

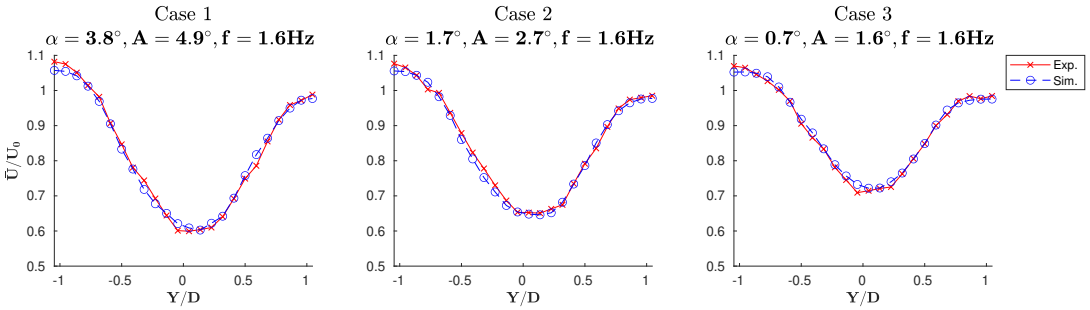

Figure 1: Turbine wake at a 5D downstream distance, for different DIC parameters.

The simulation model can capture both steady-state average values and the dynamic response of the turbines. To correctly model the oscillation of the rotor speed, the rotor moment of inertia was measured by a trifilar method [13]. The Fourier transforms of power and thrust of the first turbine for experiments and simulations were calculated, as shown in Fig. 2 for the reference case. There are peaks at multiples of the pitch excitation frequency of 1.6 Hz both for the simulation and the experiment, and the values of the peaks are in a very good agreement. Experimental measurements of both power and thrust contain high-frequency noise, which is not present in the simulations. The measured power has some low-frequency oscillations as a result of a slightly varying inflow speed, which is not modeled by CFD. However, these mismatches are at least one order of magnitude smaller compared to the peak of the response at the excitation frequency. Therefore, the CFD simulations should be able to capture turbine fatigue loads with good accuracy.

The harmonic amplitudes of power P and thrust T at the excitation frequency 1.6 Hz are shown in Table 1. These quantities are the most important contributor to fatigue loads. Here again, an excellent match between experiments and simulations can be appreciated.

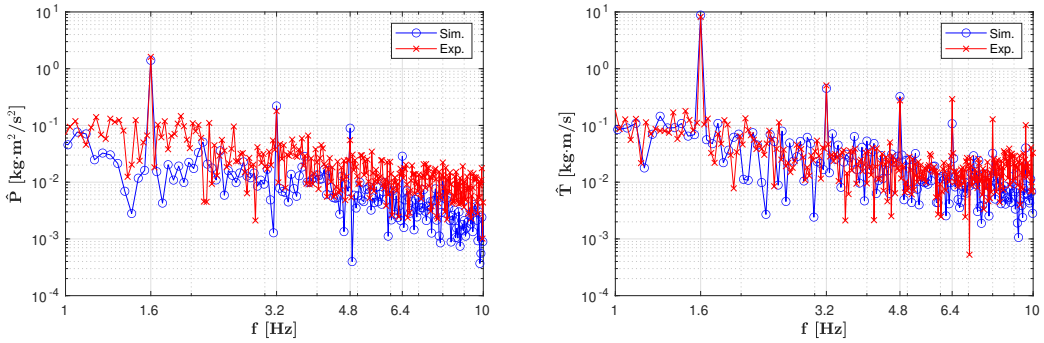

Figure 2: Power and thrust spectra of the first turbine for the reference case: $\alpha = 3.8°$, $A = 4.9°$, $f = 1.6Hz$.

Case	$A[^\circ]$	$\hat{P}_E(f_0)$ $[J]$	$\hat{P}_S(f_0)$ $[J]$	$\hat{T}_E(f_0)$ $[J]$	$\hat{T}_S(f_0)$ $[J]$
1	4.9	1.61	1.4	8.18	8.8
2	2.7	0.95	0.9	5.16	6.14
3	1.6	0.49	0.53	2.98	3.84

Table 1: Amplitudes of the power and thrust harmonics at the pitch excitation frequency $f_0 = 1.6$ Hz, for experiments (subscript E) and simulations (subscript S).

3.2. CFD validation: the reference case

Next, DIC was applied to the first turbine in a cluster of three aligned machines. This subsection shows the results for the reference DIC case. Figure 3 shows the time histories of the various quantities. Table 2 shows the mean values and the harmonic amplitudes at the excitation frequency of power, rotor speed and thrust for the same case. The match of all quantities between experiments and simulations is good. The aforementioned low frequency oscillation of power on the first turbine is clearly visible. For all other cases with different DIC parameters, a comparable match was achieved, similarly to the case presented here.

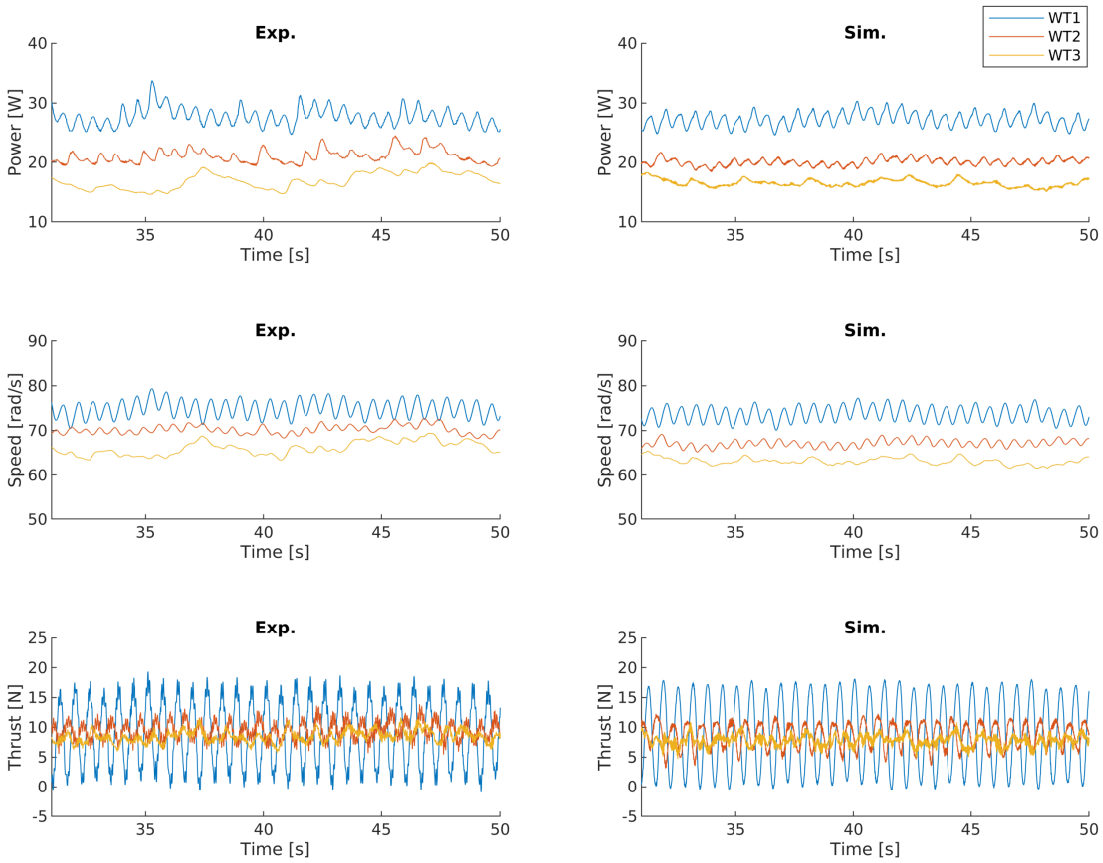

Figure 3: Power, speed and thrust time histories of the three turbines for the reference case ($\alpha = 3.8^\circ$, $A = 4.9^\circ$, $f = 1.6Hz$).

Quantity	Unit	WT1		WT2		WT3	
		Exp.	Sim.	Exp.	Sim.	Exp.	Sim.
$\bar{P}$	W	28.0	27.3	21.1	20.0	16.2	16.7
$\hat{P}(f_0)$	J	1.61	1.40	0.64	0.55	0.12	0.09
$\bar{\Omega}$	rad/s	74.8	73.7	70.1	67.1	65.3	63.4
$\hat{\Omega}(f_0)$	rad	2.39	2.19	0.69	0.91	0.18	0.13
$\bar{T}$	N	9.05	8.99	9.49	8.70	8.27	7.85
$\hat{T}(f_0)$	$kg \cdot m/s$	8.17	8.80	1.8	2.82	0.5	0.41

Table 2: Comparison between experiments and simulations of the mean power $\bar{P}$, speed $\bar{\Omega}$ and thrust $\bar{T}$ and harmonic amplitudes $\hat{P}$, $\hat{\Omega}$, $\hat{T}$ at $f_0 = 1.6$ Hz for the reference case. WT1, WT2 and WT3 denote the first, intermediate and last turbines, repectively.

3.3. CFD validation: frequency sweep

A group of experiments with the same collective pitch angle $\alpha = 0.7°$, similar pitch amplitude A (between 1.5° and 2.0°) but different frequencies f was then analyzed. The wind farm power coefficient ΣC_P, defined as the sum of the individual wind turbine power coefficients, is plotted as a function of pitch frequency f in Fig. 4. Results are normalized with the wind farm power coefficient without DIC, noted ΣC_{P0}. Except for one experimental outlier at 1 Hz, the trends of simulations and experiments match well, and the optimal frequency is shown to be between 1.5 Hz and 2.3 Hz, since such frequency triggers the natural instability in the wake [2].

A large number of experimental observations was conducted for varying frequencies and amplitudes. Considering all cases, the correlation coefficient between the simulated and experimental wind farm power coefficients is 0.86. Based on this extensive set of results, the CFD model appears to be capable of representing the physical phenomena at play with a good level of fidelity.

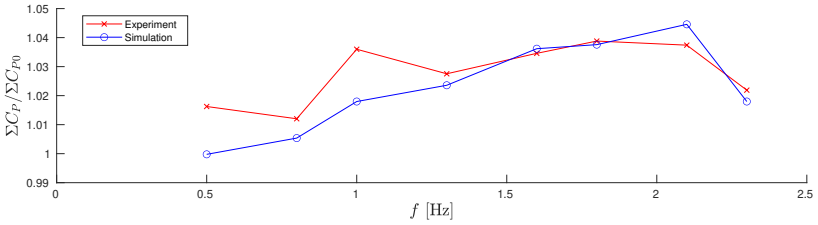

Figure 4: Wind farm power coefficient as a function of dynamic pitch frequency.

The gain obtained by employing DIC is a relatively small quantity of around 3% for the current wind farm layout. It is difficult to precisely investigate such a small difference only with experiments because of measurement uncertainties. Although the inflow condition in the wind tunnel can be controlled, each test could have slightly different mean inflow speed and wind shear. This effect is mitigated by using a pitot tube 2.3 D in front of the first-row turbine. The maximal difference of the mean flow speed measured by the pitot is about 0.7% among all tests, which indicates an excellent control of the inflow condition. However, even such a small difference results in a roughly 2% power difference, which is comparable to the maximal power gain of DIC. Hence, instead of using power, the power coefficient is used to study the effects

of DIC. Nevertheless, this relies on the measurement of a single pitot tube, which is only a single-point measurement and is itself subject to measurement errors, which could explain the small scatter of the experimental results shown in Fig. 4.

3.4. CFD exploitation: power optimization

In contrast to experiments, all CFD simulations are performed with exactly the same inflow condition for all cases, so that any change in wind farm performance in CFD can only be due to changes of DIC parameters. Hence, once the CFD tool is validated, it can be readily used to optimize the DIC parameters, which are the frequency f, collective pitch α and pitch motion amplitude A. More than 30 CFD simulations were conducted for optimization. The number of simulations is limited by their high computational cost. However, the number of data points is more than ten times the number of free variables, and as shown later, they seem sufficient to capture the behavior of the solution.

A gradient-based method was used to find the optimal parameters. The three DIC variables and the wind farm power coefficient span a 4-D space. Figure 5 shows projections of all results on three cross-sections to visualize the behavior of the normalized wind farm power coefficient $\Sigma C_P/\Sigma C_{P0}$. The maximum envelope on each plot is shown as a black curve. Although only a limited number of data points were used, the identification of the optimum should be relatively accurate since the distribution of points is relatively dense close to it.

Regarding the frequency f, there is a relatively flat peak that ranges from 1.5 Hz to 2.0 Hz, which is consistent with observations from experiments and corresponds to the natural instability of the wake, as explained in [2]. The sensitivity of the wind farm power coefficient with respect to the dynamic pitch amplitude seems to be the highest among all three DIC variables. The pitch amplitude is directly correlated with the change in thrust coefficient, and either a too large or too small value appears to be detrimental for the overall power. The collective pitch angle is optimal around the fine pitch angle 0.4° of region 2. Applying a higher collective pitch angle than the fine pitch is similar to the axial induction control, which usually does not increase wind farm power [14]. In fact, wind farm power decreases almost monotonically with respect to α.

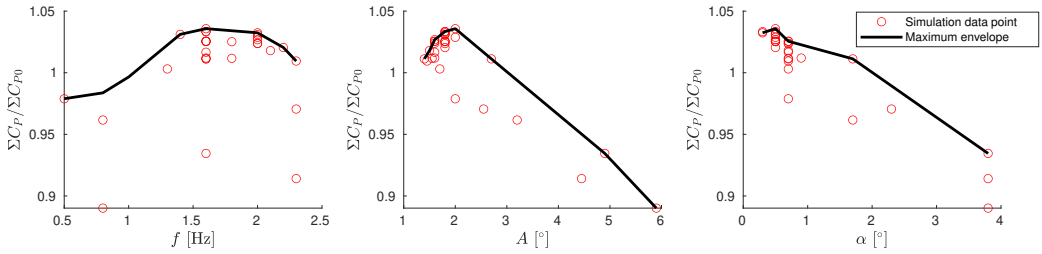

Figure 5: Behavior of wind farm power with respect to DIC parameters.

The optimal DIC parameters obtained by CFD optimization are $f = 1.6$ Hz (corresponding to a Strouhal number of 0.3), $A = 2.0°$, $\alpha = 0.5°$. The wind farm power is 3.6% higher than the baseline case. While the pitch angle is turbine-specific, the thrust coefficient has probably a more generic sense, and its amplitude is 0.274.

3.5. CFD exploitation: load analysis

The significant changes of C_T of the optimal DIC case raise concerns about fatigue loads. Damage Equivalent Loads (DELs) were computed by the rainflow algorithm [15]. Table 3 shows the DELs at blade root, at the shaft just behind the hub and at tower base for the optimal

DIC case and the baseline one. Compared to the baseline case, DIC has little influence on shaft DELs. In contrast, the DEL of the blades and tower of the front turbine increase significantly by 106% and 216% respectively, due to the periodic oscillation of thrust. For the second turbine, the increase in blade and tower DELs are 16% and 65%, caused by fluctuations in the wake speed induced by the thrust on the front turbine. Little influence is observed for the third turbine. The most critical additional loading caused by DIC is the tower fatigue of the first turbine, although this is clearly not the only problematic spot.

Case	Item	Blade DEL (Nm) or relative increase	Tower DEL (Nm) or relative increase	Shaft DEL (Nm) or relative increase
$f = 0.0Hz$	WT1	1.30	5.37	1.49
$A = 0.0°$	WT2	1.68	7.23	2.47
$\alpha = 0.4°$	WT3	1.87	7.40	2.44
$f = 1.6Hz$	WT1	+106%	+216%	+4%
$A = 2.0°$	WT2	+16%	+65%	-2%
$\alpha = 0.5°$	WT3	+3%	+11%	+9%

Table 3: DELs of some turbine components for the baseline case and their relative increase for the optimal DIC case.

4. Conclusions

LES-ALM simulations have been performed for various operating conditions of DIC, demonstrating an excellent match with experimental measurements. The experimental and numerical results are both evidence for the power enhancement capability of DIC. CFD has been used to scan the DIC parameter space and study their effects on performance. A maximum wind farm power gain of 3.6% has been determined with CFD simulations, which corresponds to a C_T oscillation amplitude of 0.274 at a Strouhal number of 0.3. However, this power increase was obtained at the cost of an extremely significant increase in fatigue loading. A continuation of this work should verify if such a large fatigue penalty is also observed for full-scale turbines, rather than the scaled models considered here.

5. Acknowledgements

This work has been supported by the CL-WINDCON project, which receives funding from the European Union Horizon 2020 research and innovation program under grant agreement No. 727477. The authors also express their appreciation to the Leibniz Supercomputing Centre (LRZ) for providing access and computing time on the SuperMUC Petascale System.

References

[1] Munters W and Meyers J 2017 An optimal control framework for dynamic induction control of wind farms and their interaction with the atmospheric boundary layer *Phil. Trans. R. Soc. A: Math., Phys. and Engineering Sci.* **375**(2091)

[2] Munters W and Meyers J 2017 Towards practical dynamic induction control of wind farms: analysis of optimally controlled wind-farm boundary layers and sinusoidal induction control of first turbines *Wind Energy Sci.* **3**(1) 409-425

[3] Frederik J et al. 2020 Periodic dynamic induction control of wind farms: proving the potential in simulations and wind tunnel experiments *Wind Energy Sci.* 245-257

[4] Campagnolo F et al. 2016 Wind tunnel testing of a closed-loop wake deflection controller for wind farm power maximization *J. Phys.: Conf. Ser.* **753** 032006

[5] Bottasso C L et al. 2014 Wind tunnel testing of scaled wind turbine models: beyond aerodynamics *J. Wind Eng. Ind. Aerodyn.* **127** 11-28

[6] West G S and Apelt C J 1982 The effects of tunnel blockage and aspect ratio on the mean flow past a circular cylinder with Reynolds numbers between 10^4 and 10^5 *J. of Fluid Mech.* **114** 361-377
[7] Jasak H 2009 OpenFOAM: open source CFD in research and industry *Int. J. Nav. Arch. Ocean* **1**(2) 89-94
[8] Guntur S et al. 2016 FAST v8 verification and validation for a MW-scale Wind turbine with aeroelastically tailored blades *Wind Energy Symp.* 1008
[9] Fleming P et al. 2014 Evaluating techniques for redirecting turbine wakes using SOWFA *Renewable Energy* **70** 211-218
[10] Wang J et al. 2019 Wake behavior and control: comparison of LES simulations and wind tunnel measurements *Wind Energy Sci.* **4**(1) 71-88.
[11] Menter F and Yury E 2005 A scale adaptive simulation model using two-equation models 43rd *AIAA Aeros. Sci. M. and Exhibit*
[12] Wang C et al. 2018 Validation of large-eddy simulation of scaled waked wind turbines in different yaw misalignment conditions *J. Phys.: Conf. Ser.* **1037**(6) 062007
[13] Hinrichsen P F 2018 Bi and trifilar suspension centering correction *Meccanica* **53**(1-2) 21-32
[14] Bartl J and Sætran L 2016 Experimental testing of axial induction based control strategies for wake control and wind farm optimization *J. Phys: Conf. Ser.* **753**(3) 032035
[15] Amzallag C et al. 1994 Standardization of the rainflow counting method for fatigue analysis *Int. J. Fatigue* **16**(4) 287-293